AMERICAN JOURNAL OF MATERIALS AND NANOTECHNOLOGY

Microstructure and Mechanical Properties of Hypo-and Hypereutectic Cast Mg/Mg_2Si Composites

Katarzyna N. Braszczynska´-Malik * and Marcin A. Malik

Faculty of Production Engineering and Materials Technology, Al, Czestochowa University of Technology, Armii Krajowej19, 42-200 Czestochowa, Poland;

Abstract: In this paper, the microstructure and mechanical properties of two magnesium matrix composites—a hypoeutectic with 1.9 wt% Mg_2Si phase and a hypereutectic with 19 wt% Mg_2Si compound—were analyzed. The investigated materials were prepared using the gravity casting method. Microstructure analyses of the fabricated composites were carried out by XRD and light microscopy. The tensile and compression strength as well as yield strength of the composites were examined in both uniaxial tensile and compression tests. The microstructure of the hypoeutectic composite was in agreement with the phase diagram and composed of primary Mg dendrites and an Mg–Mg_2Si eutectic mixture. For the hypereutectic composite, besides the primary Mg_2Si phase and eutectic mixture, additional magnesium dendrites surrounding the Mg_2Si compound were observed due to nonequilibrium solidification conditions. The composites exhibited a rise in the examined mechanical properties with an increase in the Mg_2Si weight fraction and also a higher tensile and compression strength in comparison to the pure magnesium matrix (cast in the same conditions). Additionally, analyses of fracture surfaces of the composites carried out using scanning electron microscopy (SEM + EDX) are presented.

Keywords: magnesium; composite; Mg_2Si; microstructure; mechanical properties

1. Introduction

For many years, metal matrix composites (MMCs) have been designed in many di erent systems in terms of both di erent metal matrix alloys and various types of reinforcement phase [1–5]. Among them, magnesium matrix composites are very attractive due to the especially low density of the matrix metal. Additionally, thanks to their unique combination of di erent properties such as exceptional dimensional stability and high damping capacity, specific strength and sti ness, those composites are very attractive in such applications as the aerospace, automobile or electronics industries. Typical ex situ composites, in which reinforcements are introduced from outside to the matrix alloy, comprise the biggest group of magnesium matrix composites. Many di erent magnesium matrix alloys (from the Mg–Al, Mg–Zn or Mg–rare earth systems) with various reinforced phases (various particles or fibers) such as SiC, C_{gr}, TiC, Ti, microspheres etc. have been designed and investigated in recent years [6–14].

On the other hand, in situ composites constitute a separate group, in which reinforcement is formed inside the matrix. In this group, Mg/Mg_2Si composites are typical material in which reinforcing the Mg_2Si phase is created on the inside of the matrix due to the chemical reaction between magnesium and silicon [6,15–21]. The design of magnesium matrix composites with the Mg_2Si component is based on the Mg–Si binary phase diagram (presented in Figure 1). According to this diagram, eutectic transformation proceeds at 1.48 wt% silicon, and materials from the Mg–Si system are divided into hypoeutectic, eutectic and hypereutectic. These composites can be fabricated by both powder metallurgy [22–28] and the casting process [6,29–43]. Compared to other methods, casting is a method

that can be easily adapted to the required commercial scale of production and is the most economical. Although there is a large di erence in the melting temperature of both the used elements, it is possible to dissolve silicon in liquid magnesium, which allows uniform composites with di erent weight fractions of the Mg_2Si component to be obtained.

Recently, Mg/Mg_2Si composites have been intensively investigated due to the number of properties of the Mg_2Si phase such as low density (1.99 g/cm^3), a comparatively low thermal expansion coe cient (7.5 10^{-6} K^{-1}), relatively high Young's modulus (120 GPa) and high hardness (4.5 10^9 Pa) [17–21,30–36]. It should be additionally noted that the Mg_2Si compound is also used as a reinforcing phase of aluminum matrix composites [37–43] or as a component of magnesium matrix composites with SiC or aluminosilicate microspheres [27,44,45]. However, Mg/Mg_2Si materials were most often investigated in separate experiments where composites with di erent weight fractions of silicon (i.e., the Mg_2Si phase) were analyzed. Pan Y et al. [18] described the microstructure of Mg with 8 wt% Si, whereas in works [17,29], a composite with 5 wt% Si was presented. The e ect of the Si content on low frequency damping capacities was investigated for materials with 0.3, 0.8 and 2.3 wt% Si in work [30], but in paper [16], the results for a composite with only 1 wt% Si were presented. Additionally, in many papers, the influence of a third element (such as Bi, Ce, Nd, Y, Sr, Sb) was studied in order to analyze the modification phenomenon of the Mg_2Si primary phase or eutectic mixture [15,20,21,31–35], but these investigations were also most often performed on materials with one weight fraction of the Mg_2Si compound. Recently, gradient Mg/Mg_2Si composites [46] and open cell foams [47] have also been fabricated and studied. Nevertheless, incomplete data concerning the correlation between the fabrication process, microstructure and properties of Mg/Mg_2Si composites require detailed investigations, especially for future composite design. There are also many divergent results concerning particularly the morphology of the primary Mg_2Si phase or the influence of the Si (Mg_2Si) weight fraction on the mechanical properties. In some cases, cubic or polygonal morphology of the Mg_2Si primary phase was observed [29,30], but in the other works, primary dendrites of this compound were observed in the microstructure of the composites [18,19,36]. There are also poor data describing the mechanical properties of pure Mg with Mg_2Si composites in as-cast conditions. Hu X.S. et al. [30] reported that a composite with 0.8 wt% Si exhibited the highest tensile strength (152 MPa), whereas the tensile strength decreased for a composite with 2.3 wt% Si (117 MPa). Mirshahi F. et al. [17] obtained an ultimate tensile strength equal to 95 MPa for a composite with 5 wt% Si. Higher values of the ultimate tensile strength were obtained in work [19] for hot extruded (at 623 K) composites with 3, 5 and 7 wt% Si with extrusion ratios of 6:1, 12:1 and 18:1. Unfortunately, the results for as-cast composites at the initial stage (before extrusion) were not given in this work.

In the present paper, particular investigations of the microstructure and mechanical properties of two Mg/Mg_2Si composites are presented. Hypoeutectic and hypereutectic composites were gravity cast in the same conditions, and the influence of the silicon weight fraction on the properties of the composites tested in both uniaxial tensile and compression tests (also in comparison with pure magnesium) was shown.

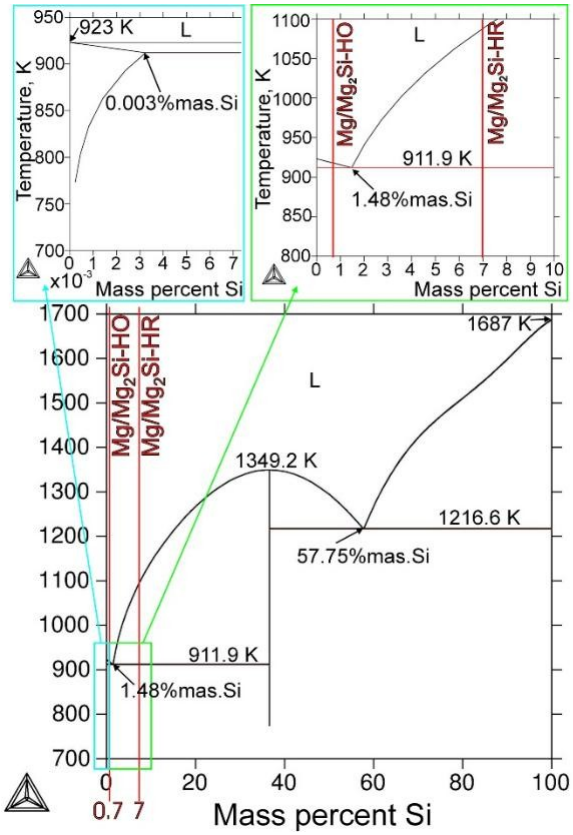

Figure1[1]. Mg–Si[Si] phase diagram (calculated in[in] Thermo-Calc Software;Database: COST2 [[48])48.

2. Materials and Methods

In the present paper, particular investigations of the microstructure and mechanical properties of twoTechnicallyMg/Mg2Sipurecompositesmagnesiumarepresentedandpure. Hypoeutecticsiliconinthe formandhypereutecofaningoticandcompositespowder, respectively,weregravity werecast inusedtheinsamethisstudyconditions,.TheMgand/Mgthe2Si influencecompositesofwerethe siliconobtaiedweightbythefrcacstingon method,onthepropertwhichinvolvedesofthe introducingcomposites Sitestedpowderinbothinto uniaxialmixedmoltentensilemagnesiumandcompressioninasteeltestscrucible(also in(withcomparisoncapacitywithofaboutpure 1magnesium).5kgofmoltenwasmagnesium)shown. under a protective argon atmosphere. The chemical compositions of the prepared materials were chosen to obtain hypoeutectic and hypereutectic materials according

2. Materials and Methods

to the phase diagram (Figure 1) calculated in Thermo-Calc Software [48]. The first hypoeutectic material (called Mg/Mg Si–HO in this work) was fabricated with 0.7 wt% silicon, which corresponds Technically pure magnesium2 and pure silicon in the form of an ingot and powder, respectively, to about 1.9 wt% Mg Si in magnesium. The second hypereutectic composite (called Mg/Mg Si–HR were used in this study2. The Mg/Mg2Si composites were obtained by the casting method,2 which in this work) was fabricated with 7 wt% silicon, which corresponds to about 19 wt% Mg Si in involved introducing Si powder into mixed molten magnesium in a steel crucible (with a capacity2 of magnesium. The prepared composite melts were gravity cast in a cold steel mold, which was designed about 1.5 kg of molten magnesium) under a protective argon atmosphere. The chemical compositions for magnesium alloys and their composites (with the relatively large riser head and set of gas vents). of the prepared materials were chosen to obtain hypoeutectic and hypereutectic materials according

The phase compositions of the investigated materials were analyzed by X-ray di raction (XRD) to the phase diagram (Figure 1) calculated in Thermo-Calc Software [48]. The first hypoeutectic

using a Brucker D8 Advance di ractometer (Bruker Corporation, Billerica, MA, USA) with Cu material (called Mg/Mg2Si–HO in this work) was fabricated with 0.7 wt% silicon, which correspondsK
X-ray radiation. Reflexes from particular phases were identified according to ICDD PDF-4+ cards [49]. to about 1.9 wt% Mg2Si in magnesium. The second hypereutectic composite (called Mg/Mg2Si–HR in
The specimens for the microstructure investigations were prepared by standard metallographic this work) was fabricated with 7 wt% silicon, which corresponds to about 19 wt% Mg2Si in
procedures. To reveal the microstructure, the samples were etched in a 1% solution of HNO in magnesium. The prepared composite melts were gravity cast in a cold steel mold, which 3was
C H OH for about 60 s. The microstructures were observed with an Olympus GX51 light microscope designed25 for magnesium alloys and their composites (with the relatively large riser head and set of
(LM)gasvents)(Olumpus,. Tokyo, Japan) with di erential interface contrast (DIC).

Mechanical properties tests of the composites were carried out according to relevant ASTM The phase compositions of the investigated materials were analyzed by X-ray diffraction (XRD)
standards on a Zwick/Roell Z100 machine (Zwick Roell Group, Ulm, Germany) with a strain rate using a Brucker D8 Advance diffractometer (Bruker Corporation, Billerica, MA, USA) with CuKα X-
of 0.01 mm/s. The performed mechanical tests included experimental determination of the ultimate ray radiation. Reflexes from particular phases were identified according to ICDD PDF- 4+ cards [49].
tensile strength (UTS) and yield strength (TYS) on standard rodlike samples with a diameter of 8 mm The specimens for the microstructure investigations were prepared by standard metallographic
in a uniaxial tensile test. Compression strength (CS) and yield strength under compression (YS) procedures. To reveal the microstructure, the samples were etched in a 1% solution of HNO3 in
were determined in the uniaxial compression test on samples with a diameter of 8 mm and length C2H5OH for about 60 s. The microstructures were observed with an Olympus GX51 light microscope
(LM) (Olumpus, Tokyo, Japan) with differential interface contrast (DIC).

Mechanical properties tests of the composites were carried out according to relevant ASTM standards on a Zwick/Roell Z100 machine (Zwick Roell Group, Ulm, Germany) with a strain rate of 0.01 mm/s. The performed mechanical tests included experimental determination of the ultimate tensile strength (UTS) and yield strength (TYS) on standard rodlike samples with a diameter of 8 mm in a uniaxial tensile test. Compression strength (CS) and yield strength under compression (YS) were
determined in the uniaxial compression test on samples with a diameter of 8 mm and length of 12 of 12 mm. Both tests were carried out at room temperature. For comparison, the same mechanical
mm. Both tests were carried out at room temperature. For comparison, the same mechanical tests tests were performed for the used technically pure magnesium (cast in the same conditions in the
were performed for the used technically pure magnesium (cast in the same conditions in the same same mold as the fabricated composites). For each material, three samples were tested. In addition,
mold as the fabricated composites). For each material, three samples were tested. In addition, the the fracture surfaces of the investigated composites after uniaxial tensile testing were observed by
fracture surfaces of the investigated composites after uniaxial tensile testing were observed by a JEOL a JEOL JSM-6610LV scanning electron microscope (SEM) (JEOL Ltd., Tokyo, Japan) with an energy JSM-6610LV scanning electron microscope (SEM) (JEOL Ltd., Tokyo, Japan) with an energy dispersive X-ray spectrometer (EDX).
dispersive X-ray spectrometer (EDX).

3. Results and Discussion
3. Results and Discussion

Figure 2 shows the X-ray di raction micrographs for the Mg/Mg_2Si–HO and Mg/Mg_2Si–HR
Figure 2 shows the X-ray diffraction micrographs for the Mg/Mg2Si–HO and Mg/Mg2Si–HR fabricated composites. It confirmed that both materials were composed of Mg and Mg_2Si phases. fabricated composites. It confirmed that both materials were composed of Mg and Mg2Si phases. Additionally, the comparison of the X-ray patterns obtained for both materials revealed a distinct
Additionally, the comparison of the X-ray patterns obtained for both materials revealed a distinct increase in the reflex intensity from the Mg_2Si phase in the Mg/Mg_2Si–HR rather than in the
increase in the reflex intensity from the Mg2Si phase in the Mg/Mg2Si–HR rather than in the Mg/Mg_2 Si–HO composite, which confirmed the rise in the volume fraction of this structural constituent Mg/Mg2Si–HO composite, which confirmed the rise in the volume fraction of this structural in the material with the higher weight fraction of silicon. It should also be noted that reflexes from pure constituent in the material with the higher weight fraction of silicon. It should also be noted that silicon were not registered, confirming that all the silicon was introduced into the molten magnesium
reflexes from pure silicon were not registered, confirming that all the silicon was introduced into the and created the Mg_2Si phase.
molten magnesium and created the Mg2Si phase.

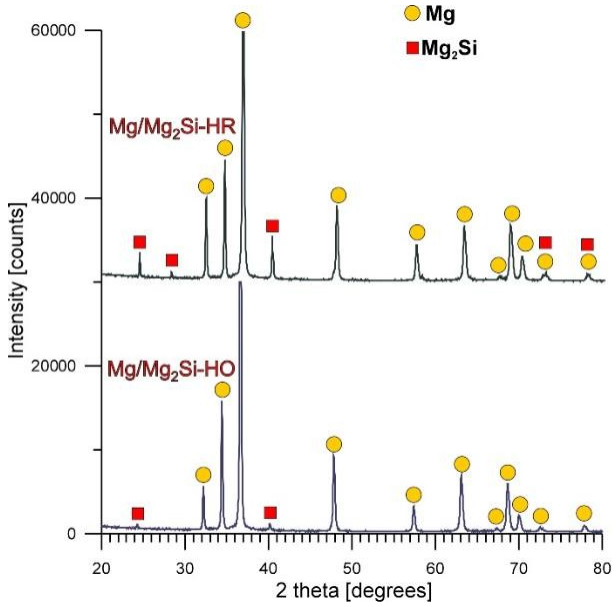

Figure 2. XX--ray diffraction patterns ofof Mg/Mg Si–HR MgMg/Mg2Si—HO and composites.2Si–HR 2
2. 2 .

in the investigated materials had irregular morphology—typical for a faceted–nonfaceted eutectic.

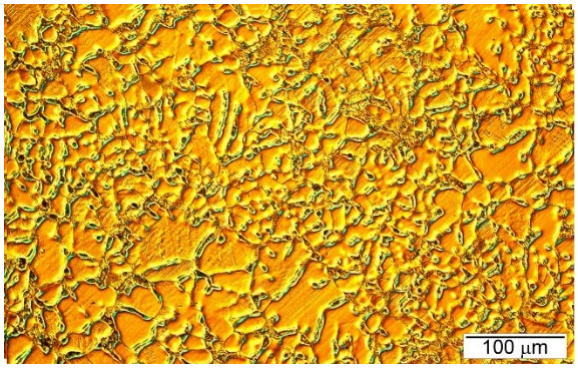

((**aa**))

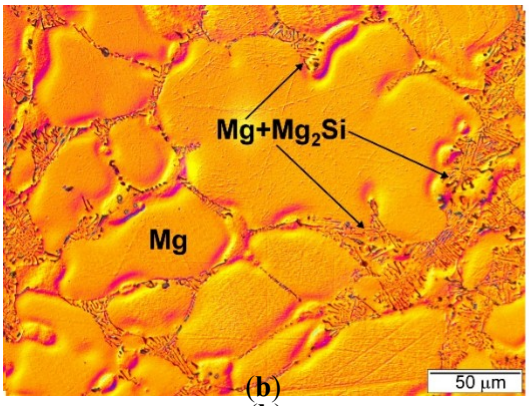

(**b**)

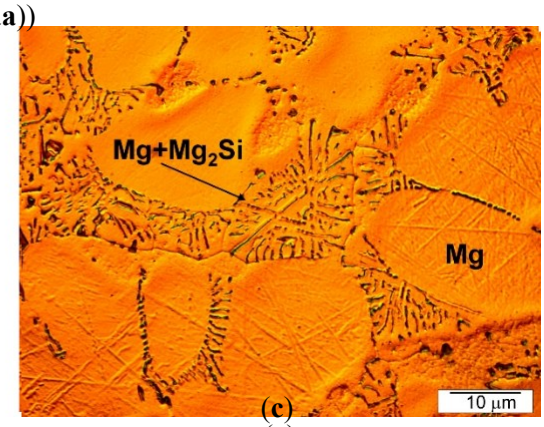

(**c**)

(**b**) (**c**)

Figure 3. Microstructure of Mg/Mg$_2$Si–HO composite at different magnifications for ((**aa**–**cc**)) three micrographs taken at different magnifications for ((**aa**—**cc**)).

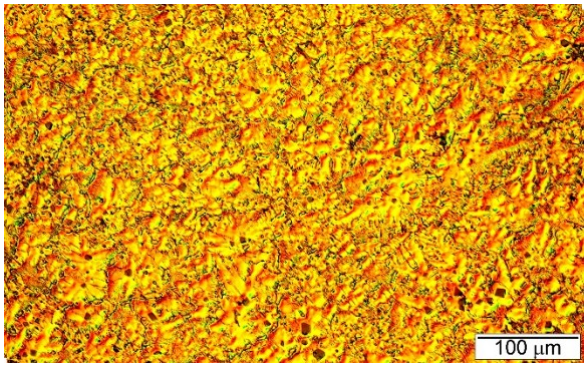

((**aa**))

Figure 4. Cont.

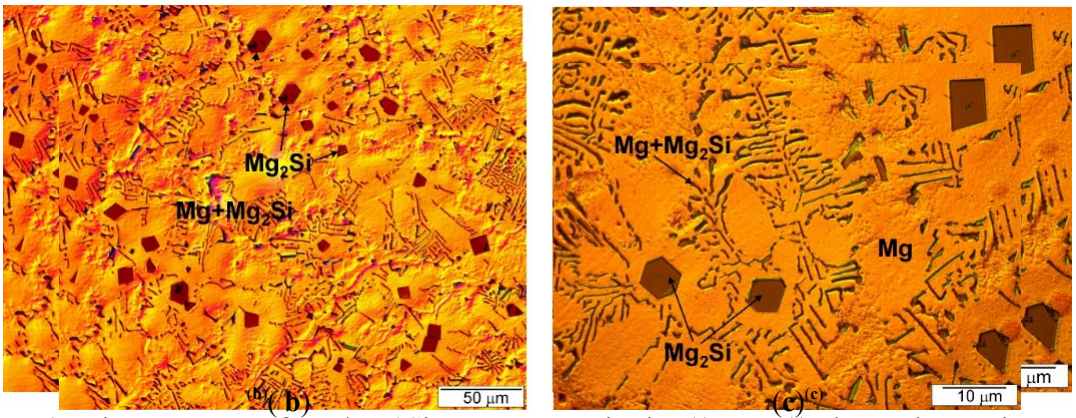

Figure 4. Microstructure of Mg/Mg2Si—HR compositesite ((**aa**—**cc**)) shows three micrographs taken at different **Figure 4.** Microstructure of Mg/Mg22Si–HR composite (**a**–**c**) shows three micrographs taken at different magnifications for Mg/Mg2Si–HR.

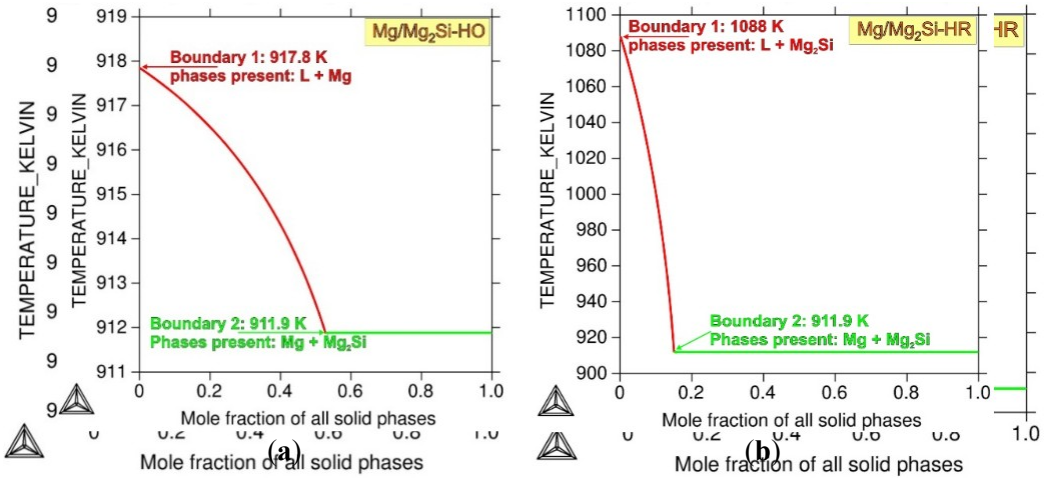

the composite (and the presence of further elements or impurities) and super-cooling during solidification (which also depends on the casting temperature). These factors need very detailed

depends on the casting temperature). These factors need very detailed studies especially in the context of impurities. It is most likely that a very small amount of surface-active third elements influenced the phase morphology, similar to the aluminum–silicon system (in which a content of up to 9 ppm phosphorus causes changes in the microstructure of hypereutectic alloys).

The formation of the primary Mg2Si phase in the Mg/Mg2Si–HR composite is in agreement with both the phase diagram (Figure 1) and the solidification curves calculated according to the Sheil

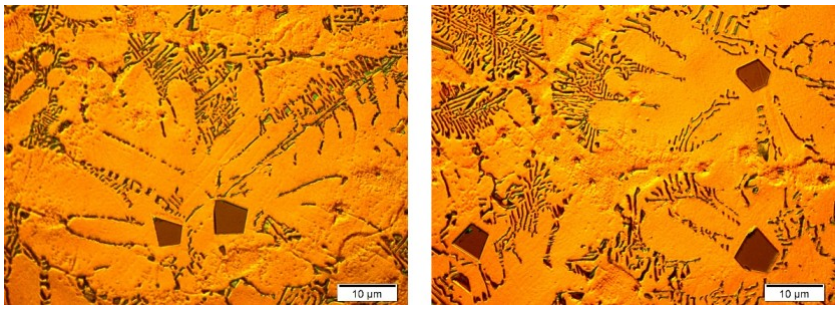

(**a**) (**b**)

Figure 6. Micrographs of Mg/Mg2Si–HR composite microstructure presenting magnesium dendrites surrounding primary Mg2Si crystals. (**a**,**b**) shows two micrographs taken from different areas of

Figure 6. Micrographs of Mg/Mg_2Si–HR composite microstructure presenting magnesium dendrites surrounding primary Mg2Si crystals. (**a**,**b**) shows two micrographs taken from different areas of

tensile test for both composites and compared with those obtained for technically pure magnesium cast in the same conditions. The analogical results presenting the compression strength (CS) and yield strength (YS) values obtained in the uniaxial compression test are shown in Figure 8b. Both the

fabricated composites exhibited higher mechanical properties than technically pure magnesium. The obtained results of the ultimate tensile strength of both the investigated composites were also

alloy[46]. [50] and significantly higher than the one obtained by the gradient composite (about 200 MPa) [46].

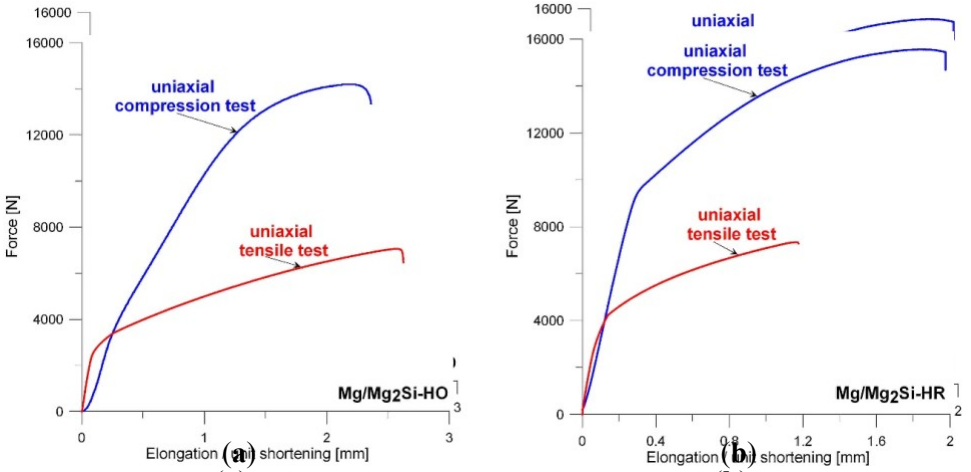

Figure 7. Representative tension and compression curves for the Mg/Mg2Si–HO (**a**) and Mg/Mg2Si–HR composites (**b**).

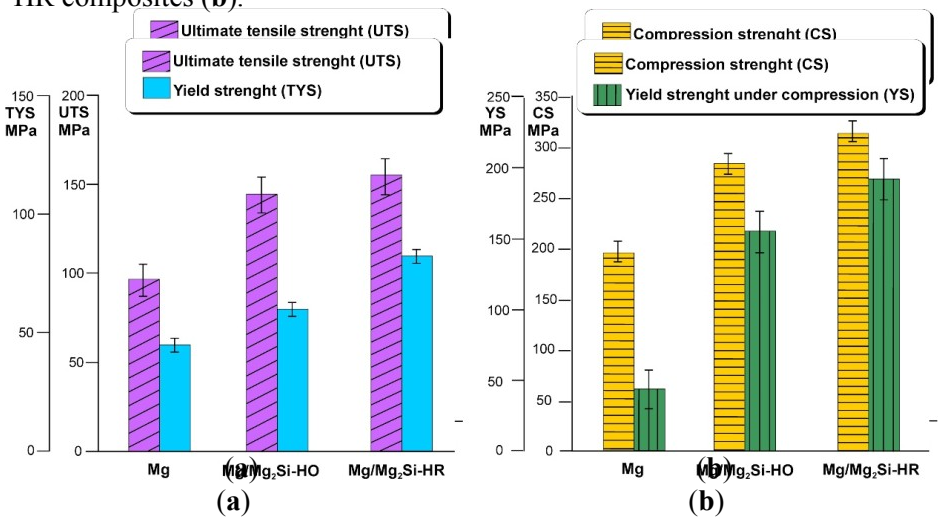

Figure 8. Average values of ultimate tensile strength (UTS) and yield strength (TYS) (**a**), compression strength (CS) and yield strength under compression (YS) (**b**) for Mg/Mg_2Si–HO and Mg/Mg_2Si–HR composites comprised with technically pure magnesium (with scatter of results).

visible when comparing Figure 9a,b (produced at the same magnification). The fracture surface of visible when comparing Figure 9a, b (produced at the same magnification). The fracture surface of visible when comparing Figure 9a, b (produced at the same magnification). The fracture surface of the Mg/Mg2Si–HO composite was characterized by cleavage steps, which are typical for magnesium. the Mg/Mg Si–HO composite was characterized by cleavage steps, which are typical for magnesium. the Mg/Mg^{2}Si–HO composite was characterized by cleavage steps, which are typical for magnesium. The failure 2of magnesium is usually brittle through cleavage or quasi-cleavage due to the hexagonal The failure of magnesium is usually brittle through cleavage or quasi-cleavage due to the hexagonal The failure of magnesium is usually brittle through cleavage or quasi-cleavage due to the hexagonal closed packed structure. Higher magnifications used during fracture surface observations (Figure 10) closed packed structure. Higher magnifications used during fracture surface observations (Figure 10) closed packed structure. Higher magnifications used during fracture surface observations (Figure 10) also revealed cracking through the Mg + Mg2Si eutectic.

alsoalso revealedrevealed crackingcracking throughthrough thethe MgMg ++ MgMg^{2}SiSi eutectic.eutectic.

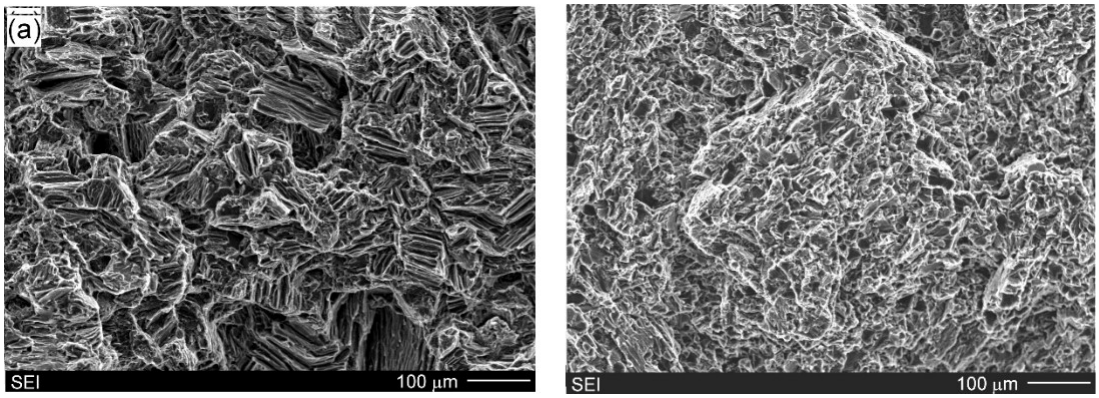

((**aa**)) ((**bb**))

Figure 9. SEM micrographs of fracture surface of Mg/Mg2Si–HO (**a**) and Mg/Mg2Si–HR (**b**) composites **Figure 9.** SE**M micrographs offracture surface of Mg/Mg$_2$Si–HO (a) and Mg/Mg$_2$Si–HR (b) composites** (after uniaxial tensile test).
(after uniaxial tensile test).

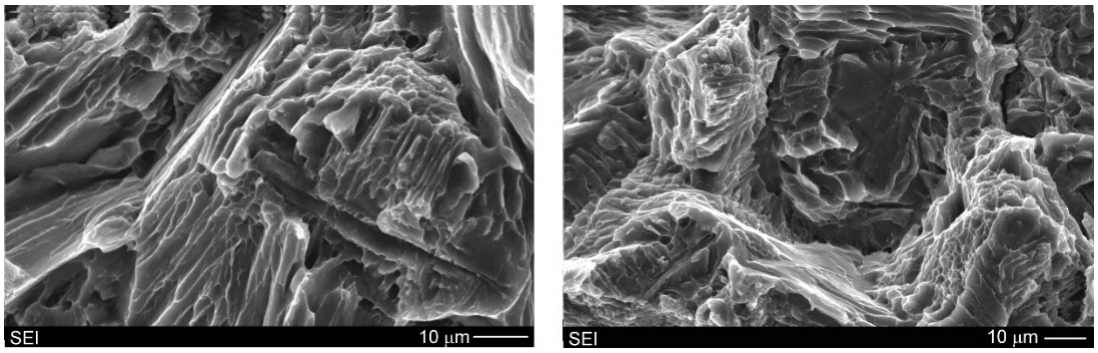

((**aa**)) ((**bb**))

Figure 10. SEM micrographs of Mg/Mg2Si–HO composite fracture surfaces illustrating cracking **Figure 10..** SE**M micrographsrs off Mg/Mg**2Si—HO co**m**posite fr**actu**re **surfaces illustrating cracking**

of the material investigated in the present study did not indicate this mechanism in the Mg/Mgg22Si— HR compositeposite.. The micrographs presented in Figuress 11c,d,d and 12 show that the cracking process
with the propagation of secondary cracks. All the Mg2Si phases designated as 1–3 in Figure 11c and as proceeded through the Mg22Si with the propagation of secondary cracks.. All the Mg22Si phases 1–2 in Figure 12a had visible e ects of brittle cracking. The presented SEM results also indicate that designated as 11—33 in Figure 11c and as 11—22 in Figure 12a had visible effects of brittle cracking.. The primary Mg2Si crystals and the surrounding magnesium phase were strongly connected, which could presented SEM results also indicate that primaryary Mg22Si crystals and the surrounding magnesium also be an additional argument for the heterogeneous nucleation of magnesium dendrites on the Mg2Si phase were strongly connected, which could also be an additional argumentent for the heterogeneous
phase. The magnesium dendrite surrounding the Mg2Si cracked particle (described as 3) is especially nucleation of magnesium dendrites on the Mg22Si phase.. The magnesium dendrite surrounding the visible in Figure 11.
Mg22Si cracked particle (described as 3) isis especially visible in Figure 11..

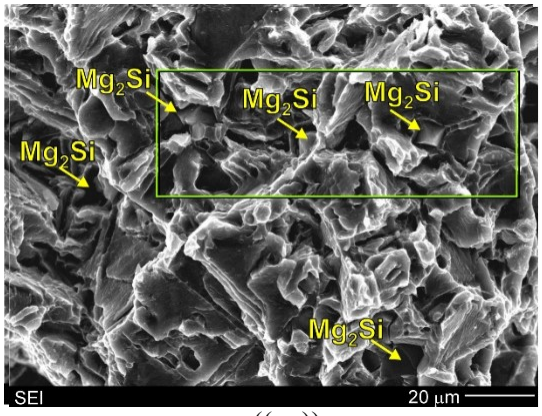

((**aa**))

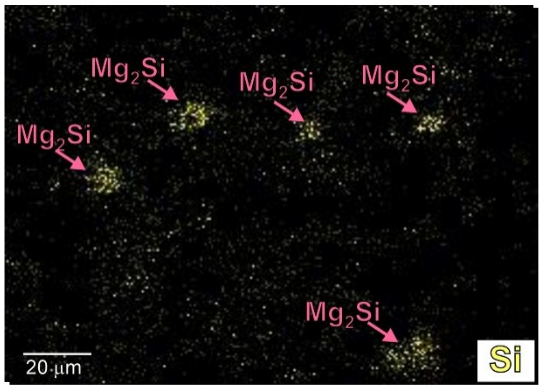

((**bb**))

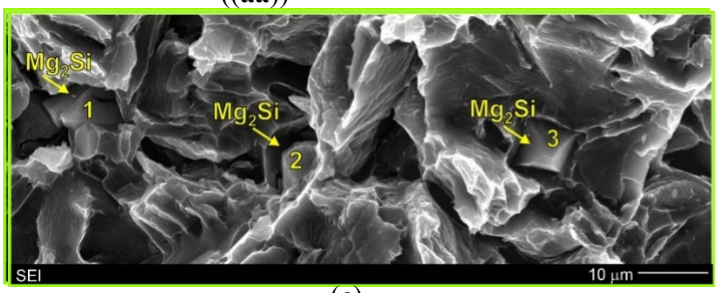

(**c**)

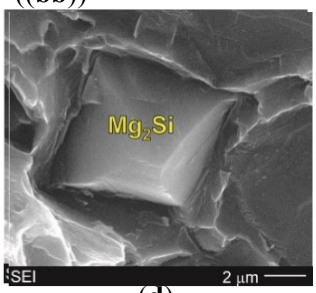

(**d**)

(**c**)

(**d**)

Figure1. of 2Si– ofMg/Mg2Si–
(**a**) (**b**), adequate of in silicon
(**c**) of 2Si
(**d**).

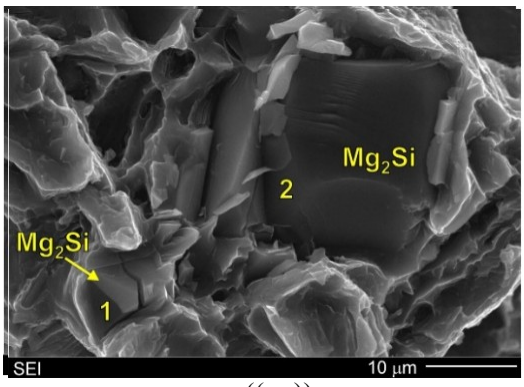

((**aa**))

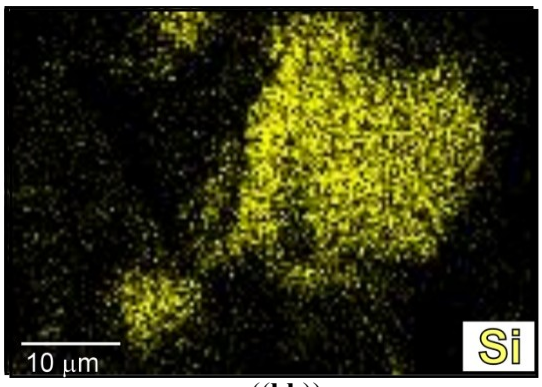

((**bb**))

Figure 12.. SEM micrographs ofof Mg/Mg22SiSi—HR composite ofof fracture surfaces (after uniaxial tensile **Figure 12.** SEM micrographs of Mg/Mg_2Si–HR composite of fracture surfaces (after uniaxial tensile test) ((**aa**)) with adequate silicon surface distribution (EDX) ((**bb**)).. test) (**a**) with adequate silicon surface distribution (EDX) (**b**).

1 Magnesium matrix composites with 1.9 and 19 wt% Mg_2Si phase were successfully fabricated by the casting method.
2 The microstructure of the material with 1.9 wt% Mg_2Si consisted of primary magnesium dendrites and an Mg + Mg_2Si eutectic mixture, whereas the composite with 19 wt% Mg_2Si exhibited a primary polygonal Mg_2Si compound surrounded by magnesium dendrites and eutectic.
3 The composites exhibited a rise in tensile and yield strength in both the tensile and compression tests with an increase in the weight fraction of the Mg_2Si phase.
4 The fracture surface observations revealed that during the uniaxial tensile test, the cracking process of the fabricated composites proceeded through all structural constituents.

Author Contributions: Conceptualization, K.N.B.-M. and M.A.M.; methodology, K.N.B.-M. and M.A.M.; investigation, K.N.B.-M. and M.A.M.; writing—original draft preparation, K.N.B.-M. and M.A.M.; writing—review and editing, K.N.B.-M. and M.A.M. All authors have read and agreed to the published version of the manuscript.

Funding: This research received no external funding.

Conflicts of Interest: The authors declare no conflict of interest.

References

1. Kucharczyk, A.; Naplocha, K.; Tomanik, M. Processing in porous niti preforms for niti/mg composites. Arch. Metal. Mater. **2019**, 64, 747–752.
2. Dolata, A.J.; Dyzia, M.; Boczkal, S. Influence of the Sr and Mg alloying additions on the bonding between matrix and reinforcing particles in the AlSi7Mg/SiC-C_{gr} hybrid composites. Arch. Metal. Mater. **2016**, 61, 651–656. [CrossRef]
3. Dolata, A.J. Hybrid composites shaped by casting methods. Solid State Phenom. **2014**, 211, 47–52. [CrossRef]
4. Nishida, Y. Introduction to Metal Matrix Composites: Fabrication and Recycling; Springer: Tokyo, Japan, 2013. [CrossRef]
5. Chawla, N.; Chawla, K.K. Metal Matrix Composites; Springer Science + Media: New York, NY, USA, 2013. [CrossRef]
6. Braszczynska´-Malik, K.N. Magnesium Alloys and Composites on Their Matrix; Czestochowa University Publisher: Cz¸estochowa, Poland, 2017; ISBN 978-83-7193-674-6.
7. Braszczynska,´ K.N. Contribution of SiC particles to the formation of the structure of Mg-3wt %RE cast composites. Zeitschrift für Metallkunde **2003**, 94, 144–148. [CrossRef]
8. Saravanan, R.A.; Surappa, M.K. Fabrication and characterization of pure magnesium-30 vol.% SiCp particle composite. Mater. Sci. Eng. A **2000**, 276, 108–116. [CrossRef]
9. Bochenek, A.; Braszczynska,´ K.N. Structural analysis of the MgAl5 matrix—SiC particles cast composites. Mater. Sci. Eng. A **2000**, 290, 122–127. [CrossRef]
10. Braszczynska´-Malik, K.N.; Przełozy˙nska,´ E. Analyses of AM50-Tip metal-metal composite microstructure. J. Alloys Comp. **2018**, 731, 1181–1187. [CrossRef]

11. Braszczynska´-Malik, K.N.; Przełozy˙nska,´ E. The influence of Ti particles on microstructure and mechanical properties of Mg-5Al-5RE matrix alloy composite. J. Alloys Comp. **2017**, 728, 600–606. [CrossRef]
12. Godzierz, M.; Olszówka-Myalska, A. Influence of casting procedure on wear of magnesium matrix composites reinforced with carbon open-celled foam. Compos. Theory Pract. **2019**, 19, 64–70.
13. Braszczynska´-Malik, K.N.; Kamieniak, J. AZ91 magnesium matrix foam composites with fly ash cenospheres fabricated by negative pressure infiltration technique. Mater. Charact. **2017**, 128, 209–216. [CrossRef]
14. Braszczynska´-Malik, K.N.; Kamieniak, J. The role of Ni-P coating structure on fly ash cenospheres in the formation of magnesium matrix composites. Metal. Mater. Trans. A **2017**, 48A, 5649–5657. [CrossRef]
15. Chen, K.; Li, Z. E ect of co-modification by Ba and Sb on the microstructure of Mg_2Si/Mg–Zn–Si composite and mechanism. J. Alloys Comp. **2014**, 592, 196–201. [CrossRef]
16. Hu, X.S.; Wu, K.; Zheng, M.Y. E ect of heat treatment on the stability of damping capacity in hypoeutectic Mg–Si alloy. Scripta Mater. **2006**, 54, 1639–1643. [CrossRef]
17. Mirshahi, F.; Meratian, M. High temperature tensile properties of modified Mg/Mg_2Si in situ composite. Mater. Des. **2012**, 33, 557–562. [CrossRef]
18. Pan, Y.; Liu, X.; Yang, H. Microstructural formation in a hypereutectic Mg–Si alloy. Mater. Charact. **2005**, 55, 241–247. [CrossRef]
19. Mosleh, S.; Emamy, M.; Majdi, H. The e ect of Si and extrusion process on the microstructure tensile properties of Mg-Mg_2Si Composite. Procedia Mater. Sci. **2015**, 11, 79–83. [CrossRef]
20. Zheng, N.; Wang, H.Y.; Gu, Z.H.; Wang, W.; Jiang, Q.C. Development of an e ective modifier for hypereutectic Mg–Si alloys. J. Alloys Comp. **2008**, 463, L1–L4. [CrossRef]
21. Hu, J.; Tang, C.; Zhang, X.; Deng, Y. Modification of Mg_2Si in Mg-Si alloys with neodymium. Trans. Nonferrous Met. Soc. China **2013**, 23, 3161–3166. [CrossRef]
22. Seth, P.P.; Singh, N.; Singh, M.; Prakash, O.; Kumar, D. Formation of fine Mg_2Si phase in Mg-Si alloy via solid-state sintering using high energy ball milling. J. Alloys Comp. **2020**, 821, 153205. [CrossRef]
23. Niu, X.; Lu, L. Formation of magnesium silicide by mechanical alloying. Adv. Perform. Mater. **1997**, 4, 275–283. [CrossRef]
24. Sun, B.; Li, S.; Imai, H.; Umeda, J.; Kon, K. Synthesis kinetics of Mg_2Si and solid-state formation of Mg–Mg_2Si composite. Powder Tech. **2012**, 2017, 157–162. [CrossRef]
25. Lu, L.; Thong, K.K.; Gupta, M. Mg-based composite reinforced by Mg_2Si. Compos. Sci. Technol. **2003**, 63, 627–632. [CrossRef]
26. Nieroda, P.; Kolezynski, A.; Leszczynski, J.; Nieroda, J.; Pasierb, P. The structural, microstructural and thermoelectric properties of Mg_2Si synthesized by SPS method under excess Mg content conditions. J. Alloys Comp. **2019**, 775, 138–149. [CrossRef]
27. Olszówka-Myalska, A.; Wrze´sniowski, P.; Myalska, H.; Godzierz, M.; Kuc, D. Impact of the morphology of micro- and nanosized powder mixtures on the microstructure of Mg-Mg_2Si-CNT composite sinters. Materials **2019**, 12, 3242. [CrossRef] [PubMed]
28. Zhang, W.; Li, X.; Ding, D.; Gao, P. Microstructure and mechanical properties of Mg_2Si/AZ91 composites in situ synthesized by using silica fume as the Si source. J. Mater. Eng. Perform. **2018**, 27, 5300–5311. [CrossRef]
29. Mirshahi, F.; Meratian, M.; Panjepour, M. E ect of cooling rate on morphology and distribution of precipitates Mg2Si particles in Mg/Mg2Si composites, Magnesium. In Proceedings of the 8th International Conference on Magnesium Alloys and Their Applications 2009, Weimar, Germany, 26–29 October 2009; Kainer, K.U., Ed.; Wiley-VCH: Weinheim, Germany, 2010; ISBN 978-3-527-32732-4.

30. Hu, X.S.; Wu, K.; Zheng, M.Y.; Gan, W.M.; Wang, X.J. Low frequency damping capacities and mechanical properties of Mg–Si alloys. Mater. Sci. Eng. A. **2007**, 452–453, 374–379. [CrossRef]
31. Han, W.D.; Li, Y.H.; Li, X.D.; Dai, J.; Li, K. Doping and adsorption mechanism of modifying the eutectic Mg_2Si phase in magnesium alloys with rare earth elements: A first-principles study. Appl. Surf. Sci. **2020**, 503, 144331. [CrossRef]
32. Wang, Y.; Guo, X. Heterogeneous nucleation of Mg_2Si and $Mg_2(Si,Sn)$ on Mg_3Sb_2 nucleus in Mg containing Si alloys. Mater. Chem. Phys. **2019**, 223, 336–342. [CrossRef]
33. Jiang, Q.C.; Wang, H.Y.; Wang, Y.; Ma, B.X.; Wang, J.G. Modification of Mg_2Si in Mg–Si alloys with yttrium. Mater. Sci. Eng. A **2005**, 392, 130–135. [CrossRef]
34. Guo, E.J.; Ma, B.X.; Wang, L.P. Modification of Mg_2Si morphology in Mg–Si alloys with Bi. J. Mater. Proc. Tech. **2008**, 206, 161–166. [CrossRef]
35. Shin, H.C.; Son, J.; Min, B.K.; Choi, Y.S.; Cho, K.M.; Cho, D.H.; Park, I.M. The e ect of Ce on the modification of Mg_2Si phases of as-cast eutectic Mg-Si alloys. J. Alloys Comp. **2019**, 792, 59–68. [CrossRef]
36. Malik, M.; Majchrzak, K.; Braszczynska´-Malik, K.N. Microstructural analysis of AM50/Mg_2Si cast magnesium composites. Arch. Foundry Eng. **2012**, 12, 109–112. [CrossRef]
37. Wang, K.Y.; Zhao, R.D.; Wu, F.F.; Wu, X.F.; Chen, M.H.; Xiang, J.; Chen, S.H. Improving microstructure and mechanical properties of hypoeutectic Al-Mg_2Si alloy by Gd addition. J. Alloys Comp. **2020**, 813, 152178. [CrossRef]
38. Que, Z.; Wang, Y.; Fan, Z. Heterogeneous nucleation of eutectic structure in Al-Mg-Si alloys. Metal. Mater. Trans. A **2020**, 51, 2697–2702. [CrossRef]
39. Shafieizad, A.H.; Zarei-Hanzaki, A.; Abedi, H.R.; Al-Fadhalah, K.J. The Mg_2Si phase evolution during thermomechanical processing of in-situ aluminum matrix macro-composite. Mater. Sci. Eng. A **2015**, 644, 310–317. [CrossRef]
40. Zainon, F.; Ahmad, K.R.; Daud, R. The e ects of $Mg_2Si_{(p)}$ on microstructure and mechanical properties of AA332 composite. Adv. Mater. Res. **2016**, 5, 55–66. [CrossRef]
41. Chegini, M.; Shaeri, M.H.; Taghiabadi, R.; Chegini, S.; Djavanroodi, F. The correlation of microstructure and mechanical properties of in-situ Al-Mg_2Si cast composite processed by equal channel angular pressing. Materials **2019**, 12, 1553. [CrossRef]
42. Ghandvara, H.; Idris, M.H.; Abu Bakar, T.A.; Nafari, A.; Ahmad, N. Microstructural characterization,
solidification characteristics and tensile properties of Al–15%Mg_2Si–x(Gd–Sb) in-situ composite. J. Mater. Technol. **2020**, 9, 3272–3291. [CrossRef]
43. Zhu, X.; Yang, H.; Dong, X.; Ji, S. The e ects of varying Mg and Si levels on the microstructural inhomogeneity and eutectic Mg_2Si morphology in die-cast Al–Mg–Si alloys. J. Mater. Sci. **2019**, 54, 5773–5787. [CrossRef]
44. Kamieniak, J.; Braszczynska´-Malik, K.N. Problems fabricating cast magnesium matrix composites with aluminosilicate cenospheres. Compos. Theory Pract. **2014**, 14, 214–218.
45. Braszczynska´-Malik, K.N.; Kamieniak, J. Analysis of interface between components in AZ91 magnesium alloy foam composite with Ni-P coated fly ash cenospheres. J. Alloys Comp. **2017**, 720, 352–359. [CrossRef]
46. Jiang, W.; Wang, J.; Yu, W.; Ma, Y.; Guo, S. In-situ formation of a gradient Mg_2Si/Mg composite with good biocompatibility. Surf. Coat. Tech. **2019**, 361, 255–262. [CrossRef]
47. Liu, J.; Zhang, L.; Liu, S.; Han, Z.; Dong, Z. E ect of Si content on microstructure and compressive properties open cell Mg composite foams reinforced by in-situ Mg_2Si compounds. Mater. Charact. **2020**, 159, 110045. [CrossRef]
48. Thermo-Calc Software AB, TCS Mg-Based Alloys Database, Version 4.0; TCMG: Stockholm, Sweden, 2015.
49. ICDD. Powder Di raction File, PDF-4+; International Centre for Di raction Data: Pennsylvania, PA, USA,
2015. Available online: https://www.icdd.com/ (accessed on 14 August 2020).